Biomech Model Mechanobiol (2009) 8:195–208
DOI 10.1007/s10237-008-0128-z

ORIGINAL PAPER

Multi-axial mechanical properties of human trabecular bone

Liliana Rincón-Kohli · Philippe K. Zysset

Received: 6 February 2008 / Accepted: 5 June 2008 / Published online: 9 August 2008

Abstract In the context of osteoporosis, evaluation of bone fracture risk and improved design of epiphyseal bone implants rely on accurate knowledge of the mechanical properties of trabecular bone. A multi-axial loading chamber was designed, built and applied to explore the compressive multi-axial yield and strength properties of human trabecular bone from different anatomical locations. A thorough experimental protocol was elaborated for extraction of cylindrical bone samples, assessment of their morphology by micro-computed tomography and application of different mechanical tests: torsion, uni-axial traction, uni-axial compression and multi-axial compression. A total of 128 bone samples were processed through the protocol and subjected to one of the mechanical tests up to yield and failure. The elastic data were analyzed using a tensorial fabric–elasticity relationship, while the yield and strength data were analyzed with fabric-based, conewise generalized Hill criteria. For each loading mode and more importantly for the combined results, strong relationships were demonstrated between volume fraction, fabric and the elastic, yield and strength properties of human trabecular bone. Despite the reviewed limitations, the obtained results will help improve the simulation of the damage behavior of human bones and bone-implant systems using the finite element method.

L. Rincón-Kohli
Laboratory of Applied Mechanics and Reliability Analysis,
Ecole Polytechnique Fédérale de Lausanne,
1015 Lausanne, Switzerland

P. K. Zysset (✉)
Institute of Lightweight Design and Structural Biomechanics,
Vienna University of Technology (TU-Wien),
Gußhausstraße 27-29, 1040 Vienna, Austria
e-mail: philippe.zysset@tuwien.ac.at

Keywords Compression · Elasticity · Fabric · Mechanical testing · Multi-axial · Strength · Trabecular bone · Yield

1 Introduction

Trabecular bone is a highly evolved heterogeneous and anisotropic mineralized tissue that plays an important biomechanical role in osteoporotic fractures and fixation of various implants. Enclosed in compact bone at the end of epiphyses or in the core of flat and small bones, trabecular bone is subjected to multi-axial strains and stresses during physiological loading. The morphological and mechanical properties of trabecular bone have been investigated by anatomists and engineers since the end of the nineteenth century (Rauber 1876; Meyer 1867; Wolff 1892) and large efforts have been made since then to clarify the relationships between them. Trabecular bone morphology has been historically assessed microscopically on thin sections by quantitative stereology which estimated volume fraction (BV/TV) and more refined three-dimensional (3D) variables such as surface density, trabecular thickness, spacing and number (Parfitt 1984). In order to describe the extent of anisotropy, the method of mean intercept length (MIL) has been introduced on planar sections (Whitehouse 1974) and extended to 3D where its distribution was characterized by a second rank fabric tensor (Harrigan and Mann 1984). New technologies such as automated serial sectioning, micro-CT and micro-MRI have enabled assessment of trabecular morphology in three dimensions with increasing detail (Feldkamp et al. 1989; Chung et al. 1993; Rüegsegger et al. 1996). Direct methods were finally developed to perform automated histomorphometry on the resulting 3D images (Hildebrand et al. 1999). In contrast to histomorphometry, mechanical testing of

trabecular bone has not been as successful. Factors such as sample geometry, variable architecture and nonphysiological boundary conditions have lead to diverging experimental results (Odgaard and Linde 1991; Keaveny et al. 1993; Zysset et al. 1994; Zhu et al. 1994; Keaveny et al. 1997). Uni-axial mechanical compression tests were widely used to assess stiffness, strength, creep and fatigue properties of trabecular bone (Keaveny et al. 2001). Alternatively, ultrasound methods were used for measuring elastic properties with the inherent limitations of a continuum approach for wave propagation applied to a highly heterogeneous microstructure (Ashman et al. 1989; Turner et al. 1990). Work is still ongoing that attempts to clarify the effect of architecture on wave propagation in trabecular samples (Haiat et al. 2007). Finally, micro finite element (micro FE) analysis was used for computing the elastic and yield properties of trabecular bone based on 3D reconstructions (Hollister et al. 1994; Müller and Rüegsegger 1995; van Rietbergen et al. 1995; Ladd and Kinney 1998; Niebur et al. 2000, 2002; van Rietbergen 2001). It should be emphasized that bone matrix properties must be assumed in these models and that only recently a proper validation of the method was achieved for elasticity (Chevalier et al. 2007). Nevertheless, a super-ellipsoid yield criterion independent of volume fraction (strain-based) was proposed and its material constants identified for three samples from the proximal femur (Bayraktar et al. 2004). Compared to what is known about uni-axial and elastic or yield properties, much less is known about multi-axial strength which is the most relevant variable in view of osteoporotic bone fractures (Stone et al. 1983). The first study to test a complete multiaxial strength criterion was made on bovine trabecular bone with high volume fraction. The observed failure behavior was not found to be properly described by a transverse isotropic Tsai-Wu criterion but variations in microarchitecture were not taken into account (Keaveny et al. 1999). In contrast, a cellular solid strength criterion was found to be appropriate for axial-shear failure properties of bovine tibial trabecular bone (Fenech and Keaveny 1999). Morphology–mechanical properties relationships based on volume fraction and fabric were pioneered by Cowin (1985, 1986). Alternative relationships and the application to elastic properties of human trabecular bone were reviewed by Zysset (2003). The first fabric-based strength criterion was inspired from the Tsai-Wu model for composite materials and expressed all material constants as functions of volume fraction and fabric eigenvalues (Cowin 1986). An alternative fabric based failure model was proposed which was insensitive to hydrostatic pressure (Pietruszak et al. 1999). Finally, a conewise generalized quadratic Hill criterion was recently formulated that, like the Tsai-Wu model, accounts for distinct properties in compression and tension (Zysset and Rincón-Kohli 2006). To the best of our knowledge, no experimental program was undertaken to identify the material constants for human trabecular bone of any of these models. In this context, the goal of this work was to develop a multi-axial testing technique for human trabecular bone and, combined with uni-axial and torsion tests, to identify fabric based yield and strength criteria for a collection of samples from different anatomical locations. First, a multi-axial loading chamber was developed and validated with a homogeneous polymer. A refined protocol was then designed to manufacture cylindrical bone specimens along their principal trabecular orientation. Morphology of these samples was then quantified by means of micro-CT. Based on volume fraction and degree of anisotropy, the bone samples with acceptable alignment were assigned to one of the following tests: uni-axial traction, torsion, uni-axial compression or three axisymmetric triaxial compression tests with three distinct axial/radial stress ratios, respectively. Monotonic proportional loads up to failure were applied for each loading mode. All elastic, yield and strength properties were analyzed in terms of volume fraction and fabric. Finally, the constants of the yield and strength criteria by Zysset and Rincón-Kohli (2006) were identified for human trabecular bone.

2 Materials amd methods

2.1 Materials

Trabecular bone samples were obtained from 12 human cadavers (7 females, 5 males) with age ranging from 30 to 89 years (mean 73.5, SD 16.8). The proximal femurs, proximal tibias, distal radii and the lumbar spine were extracted from each subject if no malformations were observed. Cause of death and medical history were reviewed to ascertain the absence of bone pathologies. The bones were then stored at −26°C. In order to avoid intra-specimen heterogeneity and still satisfy the continuum assumption (Harrigan et al. 1988), a cylindrical geometry of 8 mm diameter and 10 mm length was selected. The bone epiphyses and vertebral bodies were first embedded in an aluminum mould using plaster. The principal material direction was quantified using two contact radiographs in the frontal and the sagittal plane. The moulds were then placed in a 3D positioning system on the bench of a drilling machine, and the trabecular bone samples were extracted precisely along the principal direction with a diamond-coated trephine (WMC AG, Lotzwil, Switzerland). At last, the 8 mm diameter cylindrical cores were cut to 10 mm length by means of a diamond band saw (EXAKT Apparatebau GmbH, Norderstedt, Germany). A total of 139 trabecular bone samples were obtained. The specimens were machined under copious water irrigation and then stored again at −26°C. Their exact dimensions were measured using a calliper.

2.2 Morphological analysis

All 139 trabecular bone samples were scanned in saline solution in a micro-CT (μCT20 or μCT40, Scanco Medical AG, Switzerland) with a resolution of 30 × 30 × 30 μm or 30 × 30 × 50 μm, respectively. The inner 6 mm diameter of the bone samples were then evaluated by 3D histomorphometry to avoid measuring the bone debris potentially accumulated on the sample surface during the coring process. Volume fraction (BV/TV), the second order fabric tensor based on mean intercept length (MIL) and direct structural indices such as trabecular thickness (Tb.Th*), trabecular spacing (Tb.Sp*), trabecular number (Tb.N*) and structure model index (SMI) were assessed (Hildebrand et al. 1999). Eleven cylindrical bone samples exhibiting the highest misalignment ($\alpha > 10.5°$) with respect to the principal material direction (largest fabric eigenvalue) were discarded. Based on this morphometric analysis, the remaining 128 trabecular bone samples were allocated in 16 groups of 8 samples each by dividing in quartiles the range of values of the volume fraction and the degree of anisotropy (ratio of largest over the smallest fabric eigenvalue). Unpaired t tests were used to examine differences in microstructural indices between anatomical sites.

2.3 Triaxial testing chamber for trabecular bone

A custom-made loading chamber was designed and built for triaxial testing of cancellous bone (Fig. 1). A stainless-steel custom cell was mounted on the lower part of a servohydraulic testing machine (MTS, Eden Prairie, USA), where the samples were compressed axially via a loading ram attached to a 2.5 kN external load cell (Model 662.20G-01, MTS, Eden Prairie, USA). Displacements were measured with a ±1 mm LVDT (WETA1/2 mm, HBM GmbH, Darmstadt, Germany) built into the custom chamber. A radial pressure was generated around the cylindrical samples by an external hydraulic system, controlled by an additional output channel of the testing machine. Radial pressure was measured with a 10 MPa transducer (P3MB, HBM GmbH, Darmstadt, Germany) threaded to the core of the loading chamber. An 8 mm diameter, 0.5 mm thick nitrile membrane was used to isolate the cylindrical samples from the pressurizing oil. It was calculated that this membrane reduces the pressure transmitted to the sample by 4.8%. Half of a sphere was laid on the top of the samples to counteract possible misalignments between the loading ram and the custom chamber.

For the sake of validation, five 8 mm diameter, 10 mm long elastomer samples (Adiprene) with known isotropic elastic properties were subjected to multi-axial tests. The radial pressure was increased proportionally to the axial stress for three distinct ratios (1.2, 1.9 and 4.6). The average errors

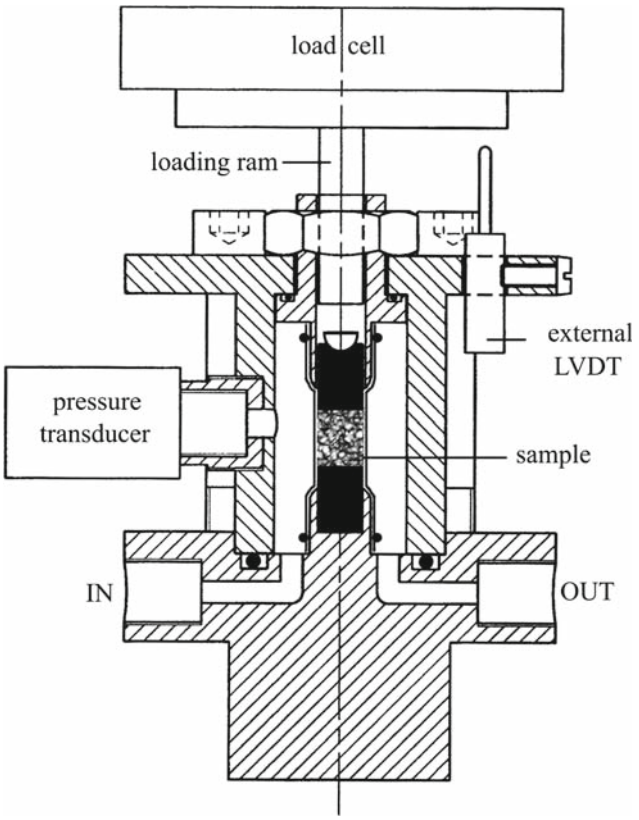

Fig. 1 Scheme of the triaxial testing chamber for trabecular bone samples. Axial stress is produced by the loading ram and radial stress is applied with pressurized oil through a membrane isolating the bone sample

between the theoretical and measured stiffnesses turned out to be 0.5, −2.2 and +4.3%. Given these satisfactory results, the contribution of the membrane and the compliance of the multi-axial loading system were assumed to be negligible.

2.4 Mechanical tests

Six series of 16 bone samples were preselected for sustaining uni-axial traction, torsion, uni-axial compression and three multi-axial compression tests, respectively. The remaining samples were devoted to a reserve group in case of embedding or testing problems. In order to avoid boundary artifacts, the ends of the cylindrical samples were embedded in polymethylmethacrylate (PMMA) cement (Technovit 3040, Heraeus Kulzer GmbH, Germany), as previously proposed by Carter et al. (1980). The specimens were kept fully wet during all mechanical tests, which detailed description can be found in Rincón-Kohli (2003). For torsion tests, the PMMA plugs were glued in hollow aluminium cylindrical end-caps (Fig. 2a). A load cell of 0.7 Nm (RTS-100, Transducer Techniques, USA) measured torque, and the RVDT of the testing

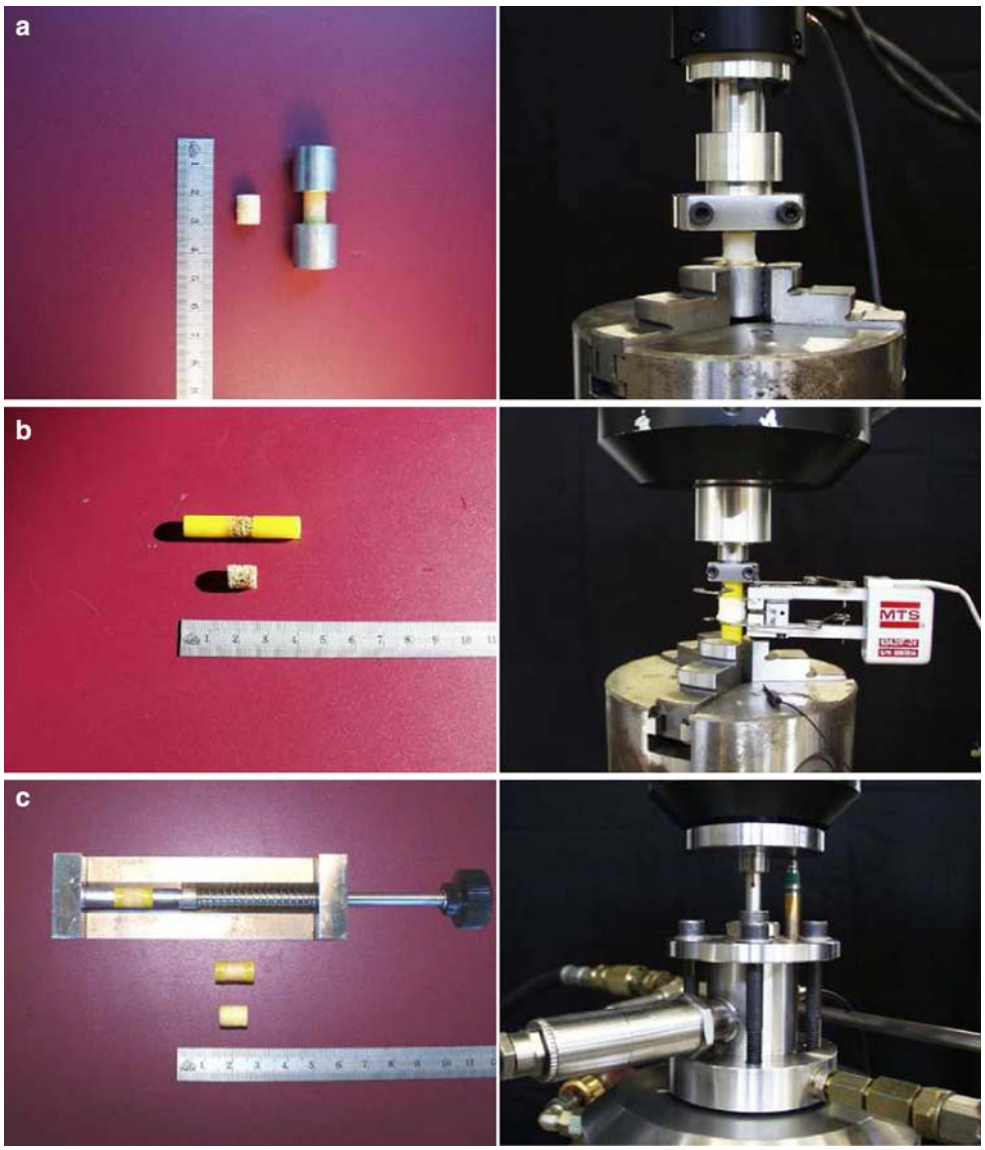

Fig. 2 Sample preparation and testing set-up for torsion (**a**), uni-axial traction (**b**), uni-axial and multi-axial compression (**c**)

machine (ADT 603.000, MTS, Eden Prairie, USA) measured the twist angle. After 12 preconditioning cycles up to 0.27%, a final ramp to failure was applied with the same strain rate of 0.047%/s. For traction tests, a 10 mm gauge extensometer was mounted on the samples fastened to the grips of the testing machine (Fig. 2b). After 12 preconditioning cycles up to $0.26 \pm 0.11\%$, a final ramp to failure was applied with the same strain rate of 0.046%/s. For uni-axial compression, the embedded samples were glued with cyanoacrylate to cylindrical aluminum end-caps (Fig. 2c). After 12 preconditioning cycles up to $0.40 \pm 0.02\%$, a final ramp to failure was applied with the same strain rate of 0.065%/s. The samples assigned to multi-axial compression underwent the same preparation protocol and preconditioning cycles described above for uni-axial compression. The computed Young's modulus allowed to determine the pressure rate that had to be applied to obtain the target axial/radial loading ratio. A monotonic proportional loading path was then applied resulting in respective mean axial/radial stress ratios of 9.44 ± 0.95, 4.59 ± 0.57 and 2.63 ± 0.25. The applied axial strain rate was identical to the one for uni-axial compression, 0.065%/s.

2.5 Tissue analysis

After mechanical testing, the PMMA plugs were cut off from the trabecular bone samples and the bone marrow was removed. Bone volume and tissue density were assessed by means of Archimede's principle (Zysset et al. 1994). Bone mineral

content was obtained by dehydrating the bone samples for the first 24 h at 40°C and converting them into ash for 24 h at 600°C in a furnace.

2.6 Data analysis

For traction and compression tests, axial nominal stress was computed as the force divided by the surface of the cylindrical bone sample and the actual deformation of bone ϵ_B was computed considering that the measured displacement was the sum of the deformation taking place in three layers: bone, bone-PMMA and PMMA alone, multiplied by their respective lengths L_B, L_{BP} and L_P.

$$\epsilon_B = \frac{\Delta L}{L_B} - \frac{\frac{\Delta F}{A}}{L_B}\left(\frac{L_{BP}}{E_{BP}} + \frac{L_P}{E_P}\right) \tag{1}$$

where ΔF is the applied force, ΔL is the total displacement and A the cross-sectional area of the sample. The elastic modulus E_P of the PMMA was 2.72 GPa, the one of the bone tissue E_{BT} assumed to be 11.4 GPa and a simple rule of mixture based on volume fraction was applied for the elastic modulus of the bone-PMMA phase:

$$E_{BP} = (\mathrm{BV/TV})E_P + (1 - \mathrm{BV/TV})E_{BT}. \tag{2}$$

For torsion tests, the torque–twist angle curves were recorded. As no local rotational displacement measurements were done, a cylindrical PMMA sample of 8 mm diameter and 41 mm length was tested in torsion with the ends glued to the same end-caps as for the bone samples. Knowing the shear modulus G_P of the PMMA (0.95 GPa), the fixation stiffness K_F was estimated. The shear strain γ_B in bone was then derived considering that the measured twist angle $\Delta\theta$ was the sum of the rotational displacement at the bone, bone-PMMA and PMMA layers:

$$\gamma_B = \left[\Delta\theta - \left(\frac{T}{K_F} + \frac{T L_{BP}}{J_{BP} G_{BP}} + \frac{T L_P}{J_P G_P}\right)\right]\frac{R_B}{L_B} \tag{3}$$

where T is the torque, R_B is the radius of the bone sample, J_{BP} and J_P are the polar moments of inertia of the bone-PMMA and the PMMA layer and G_{BP} is the shear modulus of the bone-PMMA composite that was approximated by a mixture rule similar to Eq. 2. The shear stress τ was determined from the torque-angle curve using the following equation (Nadai 1950):

$$\tau = \frac{1}{2\pi R_B}\left[\theta\frac{\mathrm{d}T}{\mathrm{d}\theta} + 3T\right] \tag{4}$$

where θ is the angle of twist per unit length. The term $\frac{\mathrm{d}T}{\mathrm{d}\theta}$ was determined by fitting a fifth-degree polynomial to the torque-angle of twist curve. The stress–strain curves obtained in the axial direction were further used to determine elastic, yield and failure properties of the trabecular bone samples. Apparent modulus, that represents the elastic modulus for uni-axial traction and compression and shear modulus for torsion test, was defined as the maximal slope of the axial stress–strain curve measured at least over a 0.3% strain range. Yield strain and yield strength were defined using the widely used 0.2% strain offset rule (Keaveny et al. 2001). Ultimate strength was the maximum stress in the axial stress–strain curve and ultimate strain was the (lowest) strain corresponding to this stress. Linear and nonlinear regressions were performed in

Table 1 Descriptive statistics of the morphological parameters of the tested bone samples from the distal radius (DR), lumbar spine (LS), proximal femur (PF) and proximal tibia (PT)

Site	Stat	BV/TV	DA	Tb.Th (mm)	Tb.Sp. (mm)	Tb.N. (mm^{-1})	SMI
DR	Min	0.056	1.372	0.114	0.687	1.212	1.560
$n = 17$	Max	0.125	2.198	0.155	0.838	1.468	2.616
	Mean	0.092	1.925	0.134	0.766	1.316	2.128
	SD	0.021	0.203	0.014	0.042	0.073	0.301
LS	Min	0.033	1.298	0.096	0.760	0.865	1.777
$n = 27$	Max	0.098	1.813	0.165	1.169	1.333	3.008
	Mean	0.060	1.477	0.124	0.939	1.081	2.428
	SD	0.020	0.113	0.015	0.105	0.122	0.381
PF	Min	0.021	1.641	0.169	0.428	1.401	−1.637
$n = 28$	Max	0.466	2.642	0.283	0.689	2.260	0.948
	Mean	0.318	1.920	0.216	0.560	1.757	−0.007
	SD	0.061	0.241	0.030	0.072	0.217	0.624
PT	Min	0.050	1.225	0.111	0.601	1.077	0.553
$n = 56$	Max	0.275	3.027	0.236	0.937	1.645	2.626
	Mean	0.130	2.114	0.149	0.728	1.375	1.680
	SD	0.050	0.393	0.028	0.080	0.130	0.497

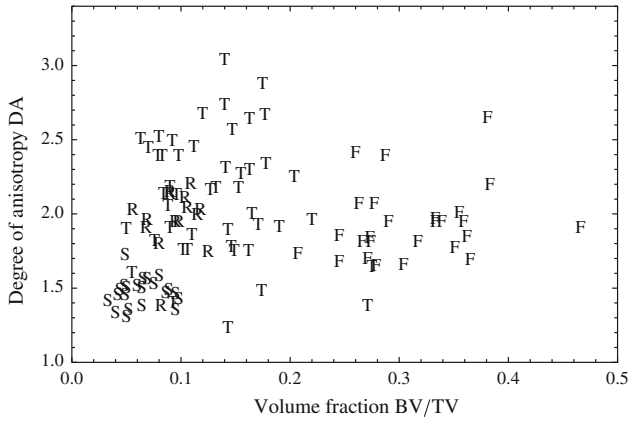

Fig. 3 Map of volume fraction and degree of anisotropy for the samples from the four anatomical regions. Proximal femur (F), lumbar spine (S), distal radius (R) and proximal tibia (T)

Mathematica (Version 6, Wolfram, USA) to fit the log transformation of the morphological and elastic data to the updated fabric-elasticity model presented in Zysset (2003):

$$E_i = E_0 \rho^k m_i^{2l} \quad \nu_{ij} = \nu_0 \frac{m_i^l}{m_j^l} \quad G_{ij} = G_0 \rho^k m_i^l m_j^l. \tag{5}$$

Similar regressions were calculated to fit the log transformation of the morphological and yield or strength data to the fabric-yield, respectively, fabric-strength model reported in Zysset and Rincón-Kohli (2006):

$$\begin{aligned} \sigma_{ii}^- &= \sigma_0^- \rho^p m_i^{2q} \quad \sigma_{ii}^+ = \sigma_0^+ \rho^p m_i^{2q} \quad \tau_{ij} = \tau_0 \rho^p m_i^q m_j^q \\ \chi_{ij}^- &= \chi_0^- \frac{m_i^{2q}}{m_j^{2q}} \quad \chi_{ij}^+ = \chi_0^+ \frac{m_i^{2q}}{m_j^{2q}} \end{aligned} \tag{6}$$

where σ_0^- and σ_0^+ are the uni-axial compressive and tensile strength, τ_0 is the shear strength, χ_0^- and χ_0^+ are interaction coefficients for a poreless ($\rho = 1$) bone material with at least cubic symmetry ($m_1 = m_2 = m_3 = 1$). Finally, multiple regressions were computed to identify the multi-axial elastic, yield and strength constants for the pooled data sets.

3 Results

3.1 Morphological properties

The microstructural indices assigned by skeletal site are summarized in Table 1. As expected, the lowest trabecular thickness and number were found in the lumbar spine (0.096 mm and 0.865 mm^{-1}) while their maxima were detected in the proximal femur (0.283 mm and 2.260 mm^{-1}). The opposite occurred for trabecular spacing, so that the lumbar spine exhibited the highest value (1.169 mm) and the proximal femur the lowest (0.428 mm). The morphological distribution in volume fraction and degree of anisotropy which was the base for the allotment of the samples is presented in Fig. 3 for the four anatomical regions. Unsurprisingly, volume fractions were significantly different between the skeletal sites ($p < 0.001$), presenting the lowest values at the lumbar spine (mean 0.06, SD 0.02) and the highest values at the proximal femur (mean 0.32, SD 0.06). As for the degree of anisotropy, a significant difference was noted between the four skeletal sites ($p < 0.001$), elucidating distinct architectures at each site. Wet tissue density ranged from 1.465 to 2.116 g/cm^3 with a mean and standard deviation of 1.841 ± 0.117 g/cm^3 while ash content ranged from 0.543 to 1.1992 g/cm^3 with a

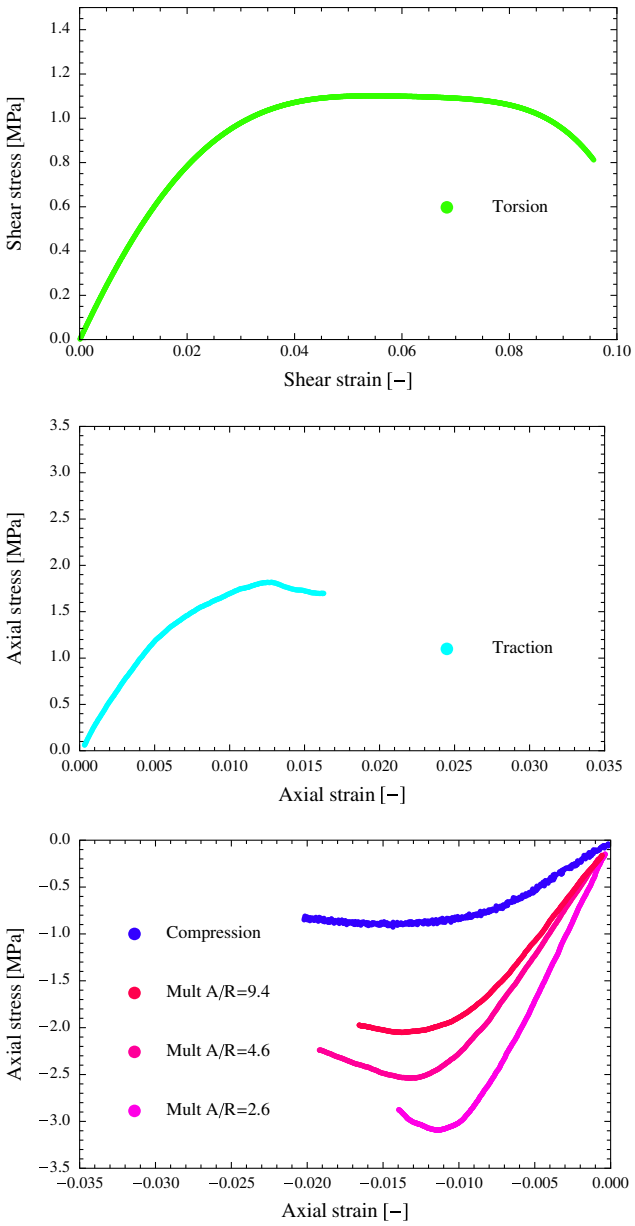

Fig. 4 Examples of stress–strain curves for the various types of mechanical tests. The volume fraction of the displayed samples are matched within the range 4.2–9.3%

mean and standard deviation of $1.010 \pm 0.117\,\mathrm{g/cm^3}$. Both tissue density and ash content were significantly different between the various skeletal sites ($p < 0.001$ in both cases), presenting the highest values at the lumbar spine. However, a linear regression between either tissue density or ash content and volume fraction (BV/TV) did not show any significant correlation ($p = 0.96$ and $p = 0.76$, respectively).

3.2 Mechanical properties

A number of strength measurements did not succeed due to torques exceeding the limits of the sensor range in torsion ($n = 4$), failure outside the extensometer gauge in tension ($n = 2$) and early sample collapse in the multi-axial chamber with the axial/radial ratio of 2.6 ($n = 10$). Reserve samples were used to repeat as many failed tests as possible. A pair of samples with very low volume fraction were suspected of prior damage and were excluded from the analysis. Typical stress–strain curves for each mechanical test are presented in Fig. 4. Descriptive statistics of apparent moduli, yield strain and stress as well as ultimate strains and strength are reported for a total of 110, respectively, 95 samples in Table 2.

3.3 Morphology versus mechanics

As shown in Fig. 5, strong relationships between volume fraction, fabric and elastic properties were found for all loading cases. The results of the regression analyses shown in Table 3 suggest distinct volume fraction and fabric exponents for the torsion data. Regression of the pooled data lead to a high correlation and a credible Poisson constant (0.181) only when a distinct elastic constant E_0 is assumed for uni-axial tension and compression. The predicted and measured yield stresses are compared in Fig. 6 and the parameters of the regression analyses are listed in Table 4. The global correlation coefficient indicates that 93% of the variations in yield stresses can be explained by volume fraction and fabric. In general, the exponent p of the yield stress was higher than

Table 2 Descriptive statistics of the mechanical variables from the uni-axial traction (UT), torsion (T), uni-axial compression (UC) and multi-axial compression (MC) tests

Site	Stat	E (MPa)	ϵ^{y} (%)	σ^{y} (MPa)	π^{y} (MPa)	ϵ^{u} (%)	σ^{u} (MPa)	π^{u} (MPa)
T	Min	17.46	0.840	0.065	–	3.440	0.297	–
$n = 17$ (14)	Max	358.2	1.430	2.648	–	8.150	5.448	–
	Mean	144.49	1.215	1.231	–	5.025	2.319	–
	SD	98.19	0.158	0.826	–	1.273	1.526	–
UT	Min	186.1	0.470	1.163	–	0.660	1.460	–
$n = 23$ (21)	Max	1759	0.830	7.373	–	0.242	9.089	–
	Mean	754.9	0.675	3.367	–	1.410	4.024	–
	SD	454.6	0.098	1.927	–	0.00432	2.340	–
UC	Min	104.5	0.890	0.837	–	1.290	0.898	–
$n = 17$	Max	1310	2.160	24.15	–	4.170	29.20	–
	Mean	597.9	1.521	8.975	–	2.307	10.16	–
	SD	401.6	0.358	7.568	–	0.773	8.916	–
MC	Min	138.3	1.020	1.177	0.148	1.340	1.314	0.328
$\lambda = 9.4$	Max	1132	2.530	25.64	2.743	4.800	30.62	4.192
$n = 16$	Mean	513.0	1.680	8.787	0.874	2.361	9.730	1.490
	SD	306.2	0.481	7.686	0.744	0.980	8.997	1.338
MC	Min	116.2	0.870	0.789	0.152	1.100	0.828	0.273
$\lambda = 4.6$	Max	1042	2.470	23.63	4.307	3.770	27.13	8.010
$n = 17$	Mean	563.4	1.546	8.834	1.730	2.295	9.788	3.103
	SD	338.2	0.482	7.701	1.473	0.969	8.792	2.631
MC	Min	121.4	0.800	0.842	0.181	0.770	1.060	0.477
$\lambda = 2.6$	Max	1112	2.420	24.75	8.804	3.290	27.70	10.17
$n = 20$ (10)	Mean	553.2	1.269	7.004	2.351	1.720	10.34	4.412
	SD	324.1	0.469	7.038	2.539	0.920	9.947	3.878

The variables are axial modulus E, the axial yield strain ϵ^{y}, yield stress σ^{y}, yield pressure π^{y}, axial ultimate strain ϵ^{u}, ultimate stress σ^{u} and ultimate pressure π^{u}. The number n in parentheses is meant for ultimate properties

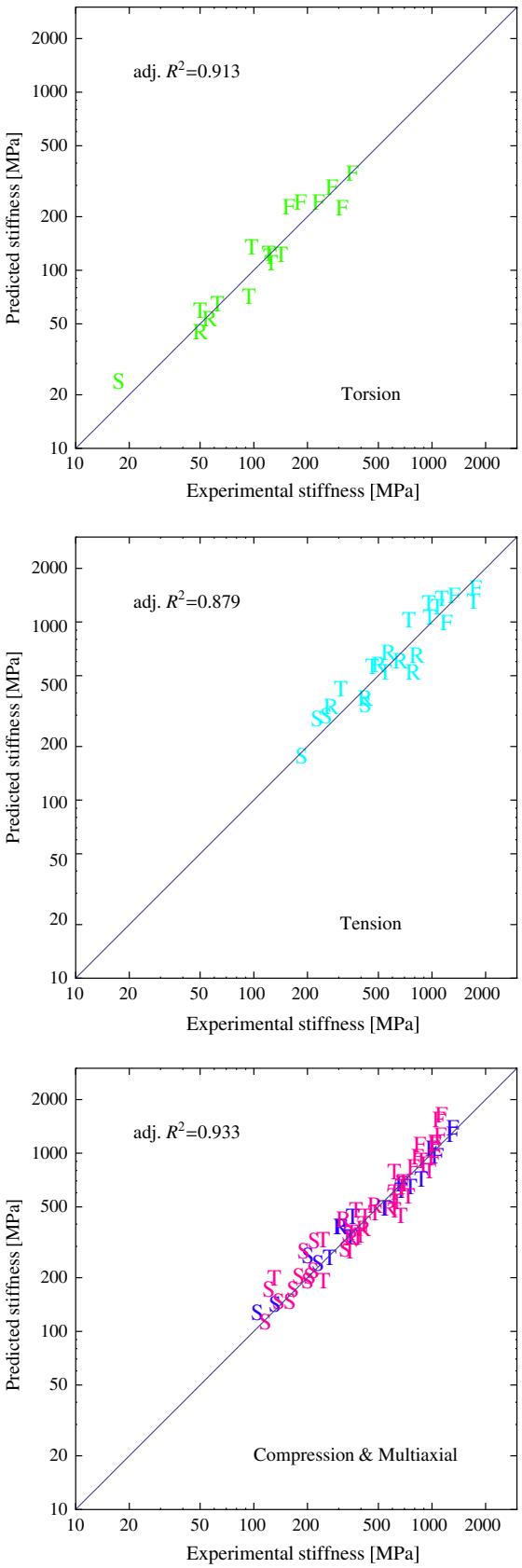

Fig. 5 Fabric–elasticity relationships for torsion, uni-axial tension and the combination of uni-axial and multi-axial compression tests

the one of the elastic modulus and the reverse was true for the exponent q. The yield strains in tension and torsion were approximately constant, while the yield strains in uni-axial and multi-axial compression increased with volume fraction (Fig. 7). The scatter of the multi-axial yield data is compared in the principal strain space and in a normalized stress space (Zysset and Rincón-Kohli 2006) that filters the variability due to volume fraction and fabric (Fig. 8). The ultimate stresses predicted with the piecewise Hill criterion and their measured counterparts are compared in Fig. 9. The parameters of the regression analyses are listed in Table 5. Similarly to the yield data, the overall coefficient of determination shows that 93% of the variations in trabecular strength can be attributed to volume fraction and fabric. As expected, the exponents p and q of the strength criterion were consistent with those of the yield criterion. Finally, the complete experimental results and the piecewise Hill criterion are presented in two sections of the normalized stress space in Fig. 10.

4 Discussion

To our knowledge this study represents the first experimental program to quantify simultaneously the morphological and multi-axial strength properties of human trabecular bone. Moreover, most of the previous experimental and numerical investigations devoted to multi-axial yield properties were applied on high density trabecular bone and the present study reports these properties for a broad range of volume fraction and fabric.

4.1 Sample preparation and morphology

A careful protocol based on two orthogonal X-rays allowed to extract the samples with an excellent alignment (<10.5°) of their principal trabecular orientation. Embedding of the sample ends in PMMA limited bending and damage accumulation responsible for boundary artifacts (Keaveny et al. 1997). The sample size was identical for all the tests in order to capture apparent mechanical properties with a similar meaning. Albeit two different μCT systems with different nominal resolutions were used for the 3D trabecular bone reconstruction, this fact was not perceived as a drawback. It has been shown that for nominal resolutions up to 50 μm, as it was used for the Scanco-20 system, the inspected structural indices remain almost constant (Müller et al. 1996). The map of Fig. 3 of volume fraction versus degree of anisotropy confirms that the samples of each anatomical locations occupy a specific area resulting from adaptation to the local mechanical requirements (Matsuura et al. 2007). The microstructural indices observed in the various anatomical locations are in line with previous studies (Hildebrand et al. 1999). The average tissue density and degree of minera-

Table 3 Fabric-elasticity material parameters for torsion (T), uni-axial tension (UT), uni-axial compression (UC), multi-axial compression (MC), the combination of the two latter as well as the combination of all tests with identical or distinct moduli in tension and compression

Tests	E_0^- (MPa)	E_0^+ (MPa)	G_0 (MPa)	ν_0	k	l	n	adj.R^2
T	–	–	404	–	1.222	9.218	17	0.913
UT	–	2,248	–	–	0.943	1.152	23	0.879
UC	1,630	–	–	–	0.976	1.124	17	0.975
MC	1,653	–	–	0.196	0.908	0.702	53	0.921
UC and MC	1,702	–	–	0.187	0.931	0.748	70	0.933
All	1,813	1,813	562	−0.003	0.927	1.000	110	0.901
All ($E_0^- \neq E_0^+$)	1,769	2,974	623	0.181	0.972	0.820	110	0.942

In the right columns, n is the number of successful tests and adj.R^2 is the squared coefficient of determination adjusted for the number of estimated parameters

lization are characteristic of nonpathological bone matrix (Gong 1964). No significant correlations between the tissue or ash densities and the volume fraction were found ($p = 0.96$ and $p = 0.76$, respectively), nevertheless, a significant differences of these measures existed between skeletal sites ($p < 0.001$). These findings were also made by Keller (1994), who found a small, but significantly higher, mean ash content for the vertebral as compared to the femoral specimens. The survey of trabecular bone composition and its similarity with values reported in the literature suggests that no mineralization-related or other bone pathology affected the samples of this study, even if the mean age of the donors was relatively high.

4.2 Elasticity

The elastic moduli in compression were found to be almost linear with volume fraction ($k \cong 1$) which contrasts with most previous uni-axial compression tests (Rice et al. 1988; Snyder and Hayes 1990; Keller 1994; Matsuura et al. 2007). We attribute this finding essentially to the high trabecular alignment in our samples which limits the bending deformation mechanism ($k = 2$, Gibson 2005) and, to a lower extent, to the embedding of the sample ends in PMMA which also restricts bending in the boundary layers. This result for perfect alignment may seem artificial, but may well be representative of physiological loading at remodeling equilibrium, i.e., when trabecular trajectories are consistent with average principal stresses. In torsion tests, the exponent of the power law with volume fraction k is somewhat higher than 1 which reflects the increased amount of bending occurring in this loading mode. Uni-axial traction tests lead to a distinct elastic constant E_0 as uni-axial compression tests which conflicts with the evidence that bone tissue exhibits identical elastic behavior in tension and compression (Gibson 2005; Keaveny et al. 2001). We believe this derives from the different strain measurement method. In traction, the extensometer is directly fixed on the sample, while the LVDT of the compression chamber is likely to include some interface compliances. The obtained Poisson constant $\nu = 0.181$ is in excellent agreement with previous micro-FE analyses (Zysset 2003). Accounting for the distinct elastic constant in traction, the overall regression of the elastic results provides a correlation coefficient $R^2 = 0.942$ which is slightly better than previous relationships obtained with micro-FE analyses (Kabel et al. 1997) and much better than previous experimental results (Snyder and Hayes 1990). The high significance of the fabric factor (typically $p < 0.0001$) in the uni-axial relationships of Table 3 together with the significantly different morphological properties among anatomical locations explain the previous finding that uni-axial modulus–volume fraction relationships depend on anatomical locations (Morgan et al. 2003).

4.3 Yield properties

The global yield constant in tension σ_0^+ was found to be 34% lower than the constant σ_0^- in compression. This is slightly higher than the 28% difference reported previously using micro-FE with the same 0.2% offset method to determine yield stress (Niebur et al. 2000). In the latter reference, the contrast in apparent compressive and tensile yield properties was induced by the distinct compressive and tensile yield properties of lamellar bone tissue used in the computation. Examining the yield stresses in uni-axial and multi-axial compression, the power exponent $p = 1.41$ related to volume fraction is somewhat higher than the exponent $k = 0.93$ for elasticity, which implies that the compressive yield strains increase with a weak power of volume fraction (Fig. 7). Since trabecular bone yields by simultaneous accumulation of plastic strain and damage (Zysset et al. 1994), the latter observation suggests that the decreasing geometrical nonlinearity associated with increasing volume fraction delays the progression of plasticity and damage in the axially oriented trabeculae. In uni-axial tension and torsion, the exponents p and k are closer which reflects that yield strains

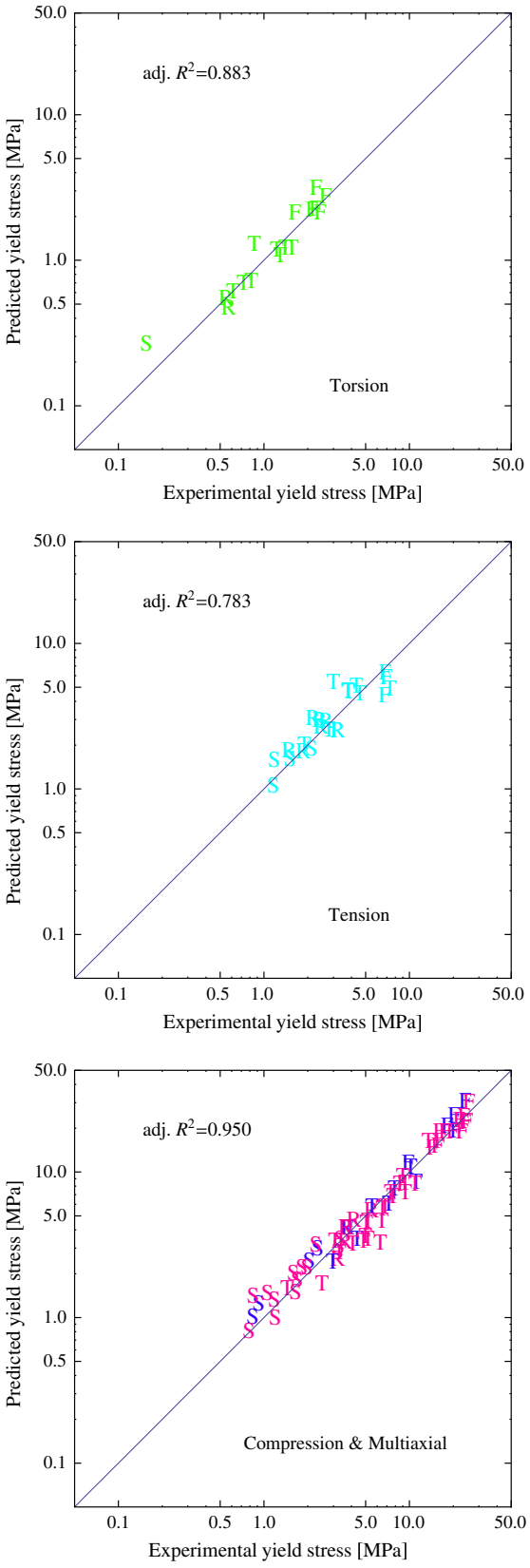

Fig. 6 Fabric–yield stress relationships for torsion, uni-axial tension and the combination of uni-axial and multi-axial compression tests

are approximately independent of volume fraction (Fig. 7). A former experimental study remained inconclusive regarding the applicability of a quadratic Tsai-Wu yield criterion for multi-axial yield properties of bovine trabecular bone (Keaveny et al. 1999). The high axial/radial stress aspect ratios, the small range of volume fraction and the limited number of samples induced a high sensitivity in the fitting parameters of the yield criterion and could, therefore, not evaluate the multi-axial behavior independently of volume fraction and fabric as done in the present work. The multi-axial yield interaction visible in Fig. 8 increases slightly the supported axial stress when a radial pressure is added. This interaction, predicted by the piecewise Hill yield criterion, is probably due to the stiffening Poisson effect of the radial pressure and discards, as expected, elastic buckling as a yield mechanism. The observed multi-axial yield interaction is also predicted by the super-ellipsoid strain criterion computed by Bayraktar et al. (2004) when transformed into stress space using linear elasticity. Their micro-FE study focussed on high volume fraction samples, did not require geometrical nonlinearity and the plastic yielding criterion, was therefore, adequately described in strain space. Nevertheless, the scattering of our experimental yield data is higher in the principal strain space as in a stress space normalized using volume fraction and fabric (Zysset and Rincón-Kohli 2006) (Fig. 8). This observation is directly related to the variability of the compressive yield strains with respect to volume fraction and fabric that emerges within a sample collection with a broad range of architectural properties. It should be mentioned that the undertaken multi-axial tests did not cover interactions between uni-axial stresses and shear, but a quadratic yield criterion such as the one used here was shown to be successful in describing this axial–shear interaction (Niebur et al. 2002).

4.4 Ultimate properties

Regarding ultimate properties, the results are qualitatively comparable to the yield behavior. The pooled uni-axial and multi-axial data were even more consistent and the fabric–strength relationship provided a remarkable correlation $R^2_{\text{adj}} = 0.97$. The global strength constant in tension σ_0^+ was 26% lower than the constant σ_0^- in compression, which trend was already shown in Keaveny et al. (1994) and reflects again the increased ultimate properties of lamellar bone tissue in compression when compared to tension (Reilly and Burstein 1975). For femoral samples with similar volume fraction, our measured strength in torsion is 25% lower than the values reported in Bruyère-Garnier et al. (1999), which is most probably due to the distinct specimen size and boundary conditions.

Table 4 Yield stress material parameters for torsion (T), uni-axial tension (UT), uni-axial compression (UC), multi-axial compression (MC), the combination of the two latter as well as all combined mechanical tests

Tests	σ_0^- (MPa)	σ_0^+ (MPa)	τ_0 (MPa)	χ_0	p	q	n	adj.R^2
T	–	–	4.06	–	1.141	7.632	17	0.883
UT	–	10.12	–	–	0.809	0.756	23	0.783
UC	34.46	–	–	–	1.327	1.223	17	0.979
MC	74.71	–	–	0.295	1.405	0.341	53	0.941
UC and MC	66.65	–	–	0.333	1.401	0.408	70	0.950
All	50.98	33.85	11.23	0.327	1.277	0.453	110	0.934

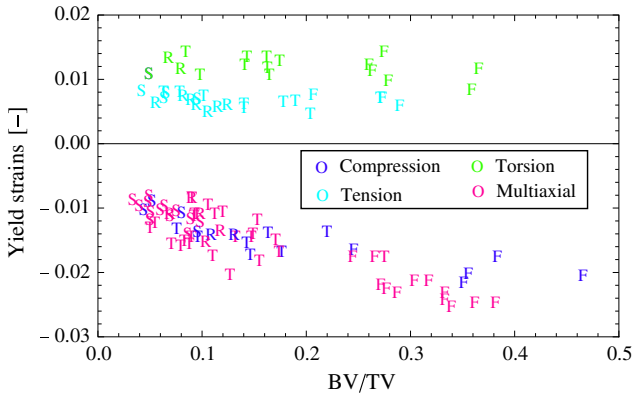

Fig. 7 Yield strains defined by the 0.2% rule in all loading modes as a function of volume fraction

The exponent $p = 1.35$ for uni-axial compression is close to 1.5 which is characteristic of plastic hinge formation in bending cell edges of an ideal foam (Gioux et al. 2000). For the multi-axial experiments, the selected axial/radial stress ratios correspond to the frequent physiological loading situation where axial stress is dominant and the radial pressure is caused by the kinematic constraint of the cortical shell. For these load paths, the ultimate axial stress was only slightly higher than for the uni-axial path which was also observed for plastic failure of aluminum and high density rigid polyurethane foams (Gioux et al. 2000; Triantafillou et al. 1989; Rincón-Kohli 2003). This suggests that the multi-axial failure mode of trabecular bone was dominated by plastic and damage yielding with subsequent hinge formation as opposed to purely elastic buckling or brittle failure. This interpretation is also consistent with time-lapsed micro-structural imaging of aluminum foam and trabecular bone, where inelastic buckling of low aspect ratio, axially oriented elements was observed in the localization zone induced by axial compression (Nazarian and Müller 2004). The compressive quadrant of the normalized strength criterion shown in Fig. 10 is qualitatively similar to the one proposed for aluminum foam in Eq. 5 of Deshpande and Fleck (2000) and Gioux et al. (2000). The multi-axial strength data shown in this work is not free of experimental limitations. The application of lateral pressure with a membrane

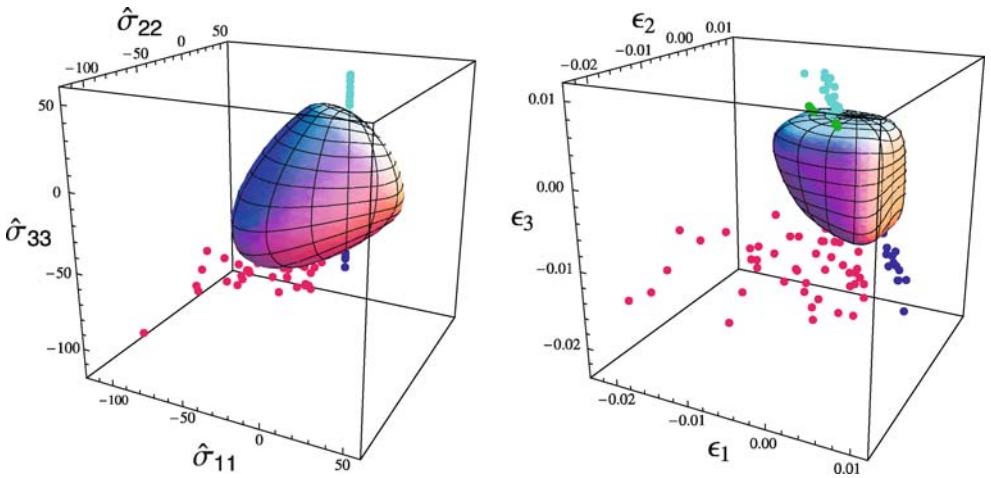

Fig. 8 Experimental yield data points in torsion (T, *green*), uni-axial traction (UT, *light blue*), uni-axial compression (UC, *dark blue*), multi-axial compression (MC, *magenta*) in the normalized stress space with the piecewise generalized Hill criterion from Zysset and Rincón-Kohli (2006) (*left*) and in the principal strain space with the super-ellipsoid criterion calibrated in Bayraktar et al. (2004) (*right*)

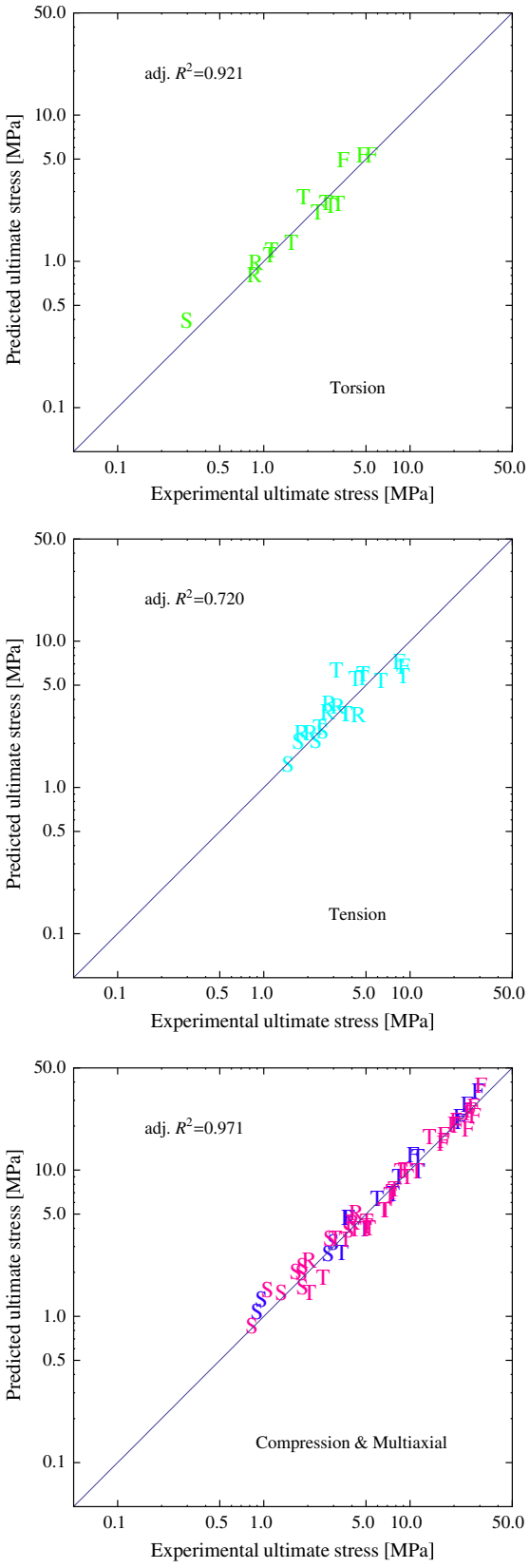

Fig. 9 Fabric–strength relationships for torsion, uni-axial tension and the combination of uni-axial and multi-axial compression tests

Table 5 Strength material parameters for torsion (T), uni-axial tension (UT), uni-axial compression (UC), multi-axial compression (MC), the combination of the two latter as well as all combined mechanical tests

Tests	σ_0^- (MPa)	σ_0^+ (MPa)	τ_0 (MPa)	χ_0	p	q	n	adj.R^2
T	–	–	9.28	–	1.372	10.49	14	0.921
UT	–	13.00	–	–	0.733	0.688	21	0.720
UC	43.82	–	–	–	1.351	1.091	17	0.980
MC	81.40	–	–	0.246	1.414	0.467	43	0.967
UC and MC	67.72	–	–	0.318	1.406	0.570	60	0.971
All	55.22	40.69	23.10	0.310	1.298	0.564	95	0.931

on small volume elements was shown to produce axial/radial stress coupling (Rincón-Kohli 2003) and boundary artifacts at the periphery of the sample (Zysset et al. 1994; Bevill et al. 2007). Finally, all apparent mechanical properties reported in this study have to be considered in the light of the selected sample size and boundary conditions. It was recently demonstrated that boundary conditions have a major impact on the apparent elastic properties of low volume fraction trabecular bone (Pahr and Zysset 2007). These boundary conditions may have an even higher impact on apparent yield and ultimate properties.

4.5 Conclusion

To conclude, phenomenological apparent yield and failure criteria based on volume fraction and fabric of human trabecular bone were identified experimentally with torsion, uni-axial tension, uni-axial compression and multi-axial tests. The samples were obtained from different anatomical locations and cover a broad range of morphological properties. Beyond the successful prediction of the orthotropic elastic properties consistent with previous work, the high coefficients of determination of the relationships between morphology and the conewise orthotropic yield and strength criteria are encouraging. The residual variability emphasizes both the inherent difficulties of manipulation and mechanical testing of excised trabecular bone samples and the random aspect of trabecular architecture that is not included in the description of volume fraction and fabric. Moreover, the influence of specimen size and boundary conditions on the apparent yield and failure properties remains unknown. In this respect, geometrically and materially nonlinear finite element analyses will help overcome these problems and identify the shape of the multi-axial yield and failure criteria along loading paths that are hardly accessible to experiments. Despite the mentioned limitations, the bulk of the presented results represents an important step towards the formulation of more reliable constitutive models for numerical simulation of damage accumulation and failure of bone or bone-implant structures.

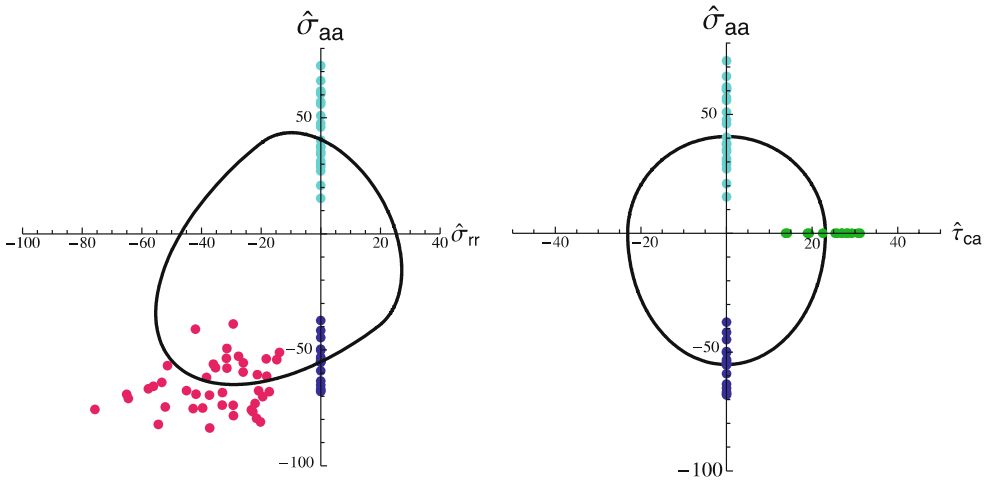

Fig. 10 Piecewise quadratic Hill strength criterion in the normalized stress space with the experimental strength data in torsion (*green*), uni-axial traction (*light blue*), uni-axial compression (*dark blue*) and multi-axial compression (*magenta*). The graph axes are normalized axial stress $\hat{\sigma}_{aa}$, radial stress $\hat{\sigma}_{rr}$ and shear stress $\hat{\tau}_{ca}$ as defined in Zysset and Rincón-Kohli (2006)

Acknowledgments The authors would like to acknowledge Professor P. Rüegsegger and Dr. Walter Pistoia for their support in computed tomography and the related morphological analysis. Further thanks to Gino Crivellari, Marc Jeanneret, Nicolas Favre, Philippe Bonhôte and Kossi Abgeviade for their contribution in the design and construction of the triaxial loading chamber. The authors acknowledge Dr. Dieter Pahr for reading the manuscript twice. This work was supported by Grant No. 32-52821.97 of the Swiss National Fund, a fellowship of the Hôpital de la Suisse Romande and a fellowship of the Ecole Polytechnique Fédérale de Lausanne.

References

Ashman RB, Rho JY, Turner CH (1989) Anatomical variation of orthotropic elastic moduli of the proximal human tibia. J Biomech 22(8/9):895–900

Bayraktar HH, Gupta A, Kwon RY, Papadopoulos P, Keaveny TM (2004) The modified super-ellipsoid yield criterion for human trabecular bone. J Biomech Eng 126:677–684

Bevill G, Easley SK, Keaveny TM (2007) Side-artifact errors in yield strength and elastic modulus for human trabecular bone and their dependence on bone volume fraction and anatomic site. J Biomech 40(15):3381–3388

Bruyère-Garnier K, Dumas R, Rumelhart C, Arlot ME (1999) Mechanical characterization in shear of human femoral cancellous bone: torsion and shear tests. Med Eng Phys 21(9):641–649

Carter DR, Schwab GH, Spengler DM (1980) Tensile fracture of cancellous bone. Acta Orthop Scand 51:733–741

Chevalier Y, Pahr D, Allmer H, Charlebois M, Zysset P (2007) Validation of a voxel-based FE method for prediction of the uniaxial apparent modulus of human trabecular bone using macroscopic mechanical tests and nanoindentation. J Biomech 40(15):3333–3340

Chung H, Wehrli FW, Williams JL, Kugelmass SD (1993) Relationship between nmr tranverse relaxation, trabecular bone architecture, and strength. Proc Natl Acad Sci USA 90:10250–10254

Cowin SC (1985) The relationship between the elasticity tensor and the fabric tensor. Mech Mater 4:137–147

Cowin SC (1986) Fabric dependence of an anisotropic strength criterion. Mech Mater 5:251

Deshpande VS, Fleck NA (2000) Isotropic constitutive modeling for metallic foams. J Mech Phys Solids 48(6):1253–1283

Feldkamp LA, Goldstein SA, Parfitt AM, Jesion G, Kleerekoper M (1989) The direct examination of three-dimensonal bone architecture in vitro by computed tomography. J Bone Miner Res 4(1):3–11

Fenech CM, Keaveny TM (1999) A cellular solid criterion for predicting the axial-shear failure properties of bovine trabecular bone. J Biomech Eng 121:414–422

Gibson LJ (2005) Biomechanics of cellular solids. J Biomech 38:377–399

Gioux G, McCormack TM, Gibson LJ (2000) Failure of aluminum foams under multiaxial loads. Int J Mech Sci 42:1097–1117

Gong JK, Arnold JS, Cohn H (1964) Composition of trabecular and cortical bone. Anat Rec 149:325–332

Haiat G, Padilla F, Peyrin F, Laugier P (2007) Variation of ultrasonic parameters with microstructure and material properties of trabecular bone: a 3d model simulation. J Bone Miner Res 22(5):665–674

Harrigan TP, Mann RW (1984) Characterization of microstructural anisotropy in orthotropic materials using a second rank tensor. J Mater Sci 19:761–767

Harrigan TP, Jasty M, Mann RW, Harris WH (1988) Limitations of the continuum assumption in cancellous bone. J Biomech 21(4):269–275

Hildebrand T, Laib A, Müller R, Dequeker J, Rüegsegger P (1999) Direct three dimensional morphometric analysis of human cancellous bone: microstructural data from spine, femur, iliac crest and calcaneus. J Bone Miner Res 14(7):1167–1174

Hollister SJ, Brennan JM, Kikuchi N (1994) A homogenization sampling procedure for calculating trabecular bone effective stiffness and tissue level stress. J Biomech 27(4):433–444

Kabel J, Van Rietbergen B, Odgaard A, Huiskes R (1997) Fabric and volume fraction can accurately predict mechanical properties for a wide range of trabecular architectures. In: Transactions of the 43rd annual meeting of the ORS, San Francisco, vol 2, p 800

Keaveny TM, Borchers RE, Gibson JG, Hayes WC (1993) Theoretical analysis of the experimental artifact in trabecular bone compressive modulus. J Biomech 26(4/5):599–607

Keaveny TM, Wachtel EF, Ford CM, Hayes WC (1994) Differences between the tensile and compressive strength of bovine tibial trabecular bone depend on modulus. J Biomech 27:1137–1146

Keaveny TM, Pinilla TP, Crawford RP, Kopperdahl DL, Lou A (1997) Systematic and random errors in compression testing of trabecular bone. J Orthop Res 15:101–110

Keaveny TM, Wachtel EF, Zadesky SP, Arramon YP (1999) Application of the Tsai-wu quadratic multiaxial failure criterion to bovine trabecular bone. J Biomech Eng 121:99–107

Keaveny TM, Morgan EF, Niebur GL, Yeh OC (2001) Biomechanics of trabecular bone. Annu Rev Biomed Eng 3:307–333

Keller TS (1994) Predicting the compressive mechanical behavior of bone. J Biomech 27(9):1159–1168

Ladd AJ, Kinney JH (1998) Numerical errors and uncertainties in finite-element modeling of trabecular bone. J Biomech 31:941–945

Matsuura M, Eckstein F, Lochmüller EM, Zysset Ph (2007) The role of fabric in the quasi-static compressive mechanical properties of human trabecular bone from various anatomical locations. Biomech Model Mechanobiol 7(1):27–42

Meyer GH (1867) Die architektur der spongiosa. Arch Anat Physiol Wiss Med 34:615–628

Morgan EF, Bayraktar HH, Keaveny TM (2003) Trabecular bone modulus–density relationships depend on anatomic site. J Biomech 36:897–904

Müller R, Rüegsegger P (1995) Three-dimensional finite element modelling of non-invasively assessed trabecular bone structures. Med Eng Phys 17(2):126–133

Müller R, Hahn M, Vogel M, Delling G, Rüegsegger P (1996) Morphometric analysis of noninvasively assessed bone biopsies: comparison of high-resolution computed tomography and histologic sections. Bone 18(3):215–220

Nadai A (1950) Torsion of a round bar. The stress-strain curve in shear. In: Nadai A (ed) Theory of flow and fracture of solids, vol 1. McGraw-Hill, New York, pp. 347–352

Nazarian A, Müller R (2004) Time-lapsed microstructural imaging of bone failure behavior. J Biomech 37(1):55–65

Niebur GL, Feldstein MJ, Yuen JC, Chen TJ, Keaveny TM (2000) High-resolution finite element models with tissue strength asymmetry accurately predict failure of trabecular bone. J Biomech 33(12):1575–1583

Niebur GL, Feldstein MJ, Keaveny TM (2002) Biaxial failure behavior of bovine tibial trabecular bone. J Biomech Eng 124(6):699–705

Odgaard A, Linde F (1991) The underestimation of Young's modulus in compressive testing of cancellous bone specimens. J Biomech 24(8):691–698

Pahr DH, Zysset PK (2007) Influence of boundary conditions on computed apparent elastic properties of cancellous bone. Biomech Model Mechanobiol doi:10.1007/s10237-007-0109-7

Parfitt AM (1984) Age-related structural changes in trabecular and cortical bone: cellular mechanisms and biomechanical consequences. Calcif Tissue Int 36:123–128

Pietruszak S, Inglis D, Pande GN (1999) A fabric-dependent fracture criterion for bone. J Biomech 32:1071–1079

Rauber AA (1876) Elastizität und Festigkeit der Knochen. Verlag Von Wilhelm Engelmann, Leipzig

Reilly DT, Burstein AH (1975) The elastic and ultimate properties of compact bone tissue. J Biomech 8:393–405

Rice JC, Cowin SC, Bowman JA (1988) On the dependence of the elasticity and strength of cancellous bone on apparent density. J Biomech 21(2):155–168

Rincón-Kohli L (2003) Identification of a multiaxial failure criterion for human trabecular bone. Ph.D., Swiss Federal Institute of Technology, Lausanne. http://library.epfl.ch/en/theses/

Rüegsegger P, Koller B, Müller R (1996) A microtomographic system for the nondestructive evaluation of bone architecture. Calcif Tissue Int 58:24–29

Snyder BD, Hayes WC (1990) Multiaxial structure–property relations in trabecular bone. In: Mow VC, Ratcliffe A, Woo SL-Y (eds) Biomechanics of diarthrodial joints. Springer, New York, pp 31–59

Stone JL, Beaupre GS, Hayes WC (1983) Multiaxial strength characteristics of trabecular bone. J Biomech 16(9):743–752

Triantafillou TC, Zhang J, Shercliff TL, Gibson LJ, Ashby MF (1989) Failure surfaces for cellular materials under multiaxial loads-II. comparison of models with experiment. Int J Mech Sci 31(9):665–678

Turner CH, Cowin SC, Rho JY, Ashman RB, Rice JC (1990) The fabric dependance of the orthotropic elastic constants of cancellous bone. J Biomech 23:549–561

van Rietbergen B (2001) Micro-FE analyses of bone: state of the art. Adv Exp Med Biol 496:21–30

van Rietbergen B, Weinans H, Huiskes R, Odgaard A (1995) A new method to determine trabecular bone elastic properties and loading using micromechanical finite-element models. J Biomech 28(1):69–81

Whitehouse WJ (1974) The quantitative morphology of anisotropic trabecular bone. J Microsc 101:153–168

Wolff J (1892) Das Gesetz der Transformation der Knochen. A. Hirchwild, Berlin

Zhu M, Keller TS, Spengler DM (1994) Effects of specimen load-bearing and free surface layers on the compressive mechanical proerties of cellular materials. J Biomech 27(1):57–66

Zysset Ph (2003) A review of fabric–elasticity relationships for human trabecular bone: theories and experiments. J Biomech 36:1469–1485

Zysset Ph, Rincón-Kohli L (2006) An alternative fabric-based yield and failure criterion for trabecular bone. In: Holzapfel GA, Ogden RW (eds) Mechanics of biological tissue. Springer, Berlin pp 457–470

Zysset Ph, Sonny M, Hayes WC (1994) Morphology–mechanical property relations in trabecular bone of the osteoarthritic proximal tibia. J Arthroplasty 9(2):203–216